Qiao et al., https://doi.org/10.1083/jcb.201607091

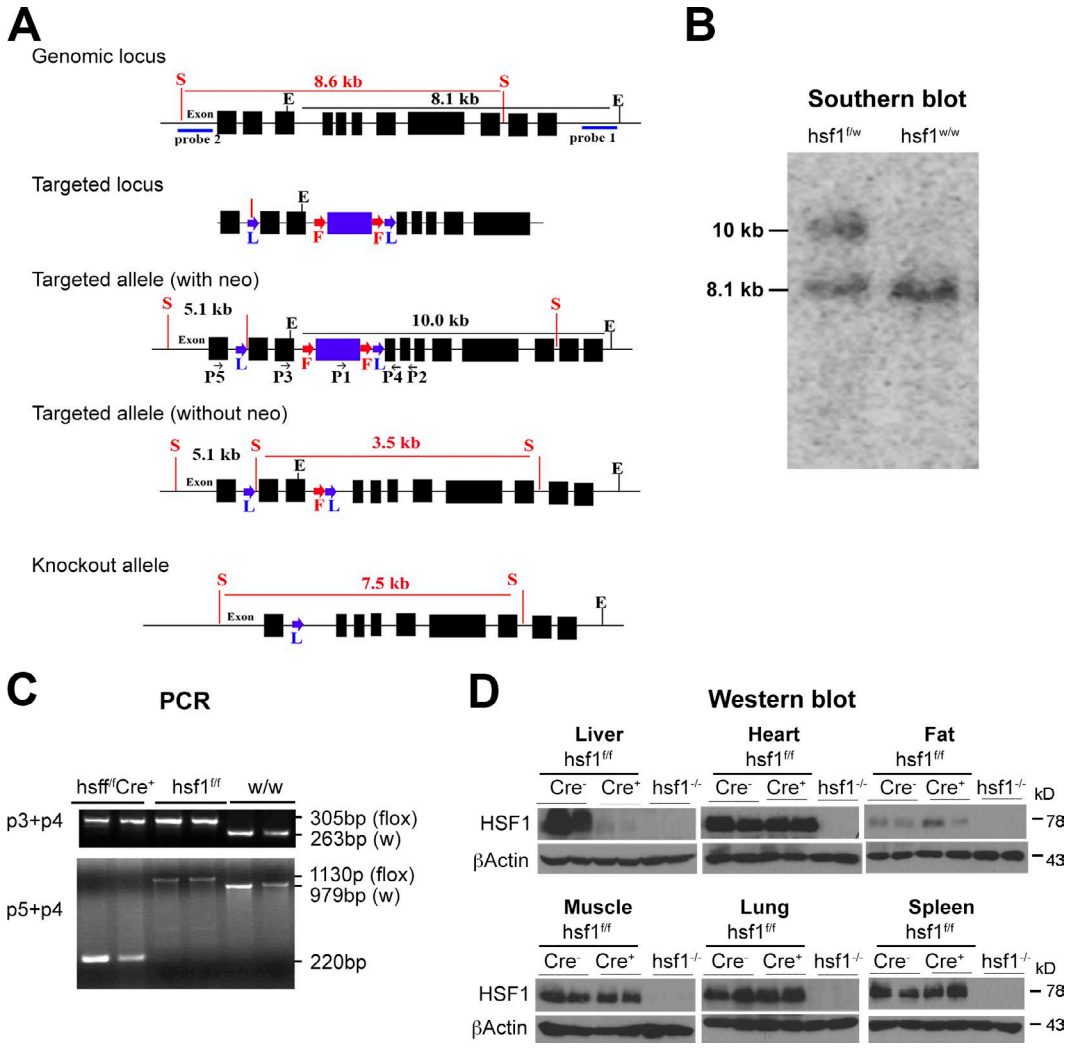

Figure S1. **Generation and characterization of mice with a conditional deletion of the *hsf1* allele.** (A) Scheme illustrating the strategy followed to generate *hsf1*$^{f/f}$ mice carrying *loxP* sites that flank exons 2 to 3 of the *hsf1* gene. The genomic locus, targeting locus, targeted allele before or after neomycin removal as well as the excised allele that disrupt HSF1 expression are shown. Neomycin gene (*neo*) is presented in blue and exons in black. F, flippase recombinase target (Frt) site. L, *loxP* site; S, SpeI; E, EcoRI. Probes for Southern blot analysis and genotyping primers (p1–p5) are indicated. Notably, *neo* is flanked by Firt sites and can be removed using flippase (Flp) transgenic mice. (B) Southern blot analysis using genomic tail DNA derived from C57BL/6 (wt/wt) or *hsf1*$^{f/w}$ (f/w) mice. DNA digested with EcoRI was hybridized with external probe 1 indicated in (A) to generate a fragment of 8.1 kb for the WT locus and 10 kb for the targeted allele. (C) PCR-based genotyping and verification of hepatocyte-specific deletion of *hsf1* allele performed with DNA isolated from tails or livers of the indicated genotypes. In the analysis performed with tail DNA, the combination of primers p3 and p4 amplifies PCR fragments of 305 and 263 bp for *hsf1*-floxed (f/f), *hsf1*$^{f/f}$-alb-cre (f/f-cre), and C57BL/6 (wt/wt) alleles, respectively (top). In PCR analysis with liver DNA preparations, the combination of primers p4 and p5 amplifies a fragment of 220 bp for the disrupted *hsf1* allele that is visible in *hsf1*$^{f/f}$-alb-cre mice and fragments of 1,130 bp and 979 bp for *hsf1*$^{f/f}$ and WT alleles, respectively. (D) Efficient inactivation of HSF1 in the indicated tissues is demonstrated by Western blot analysis in cell extracts from *hsf1*$^{f/f}$ (*hsf1*$^{f/f}$-cre^{-}) control, *hsf1*$^{f/f}$-alb-cre mice (*hsf1*$^{f/f}$-cre^{+}), or *hsf1*$^{-/-}$ mice with whole-body deletion of *hsf1* alleles. Notably, HSF1 protein is selectively lost in the liver *hsf1*$^{f/f}$-alb-cre^{+} but no other tissues, whereas *hsf1*$^{-/-}$ mice lack HSF1 from all tissues. β-Actin was used as a loading control.

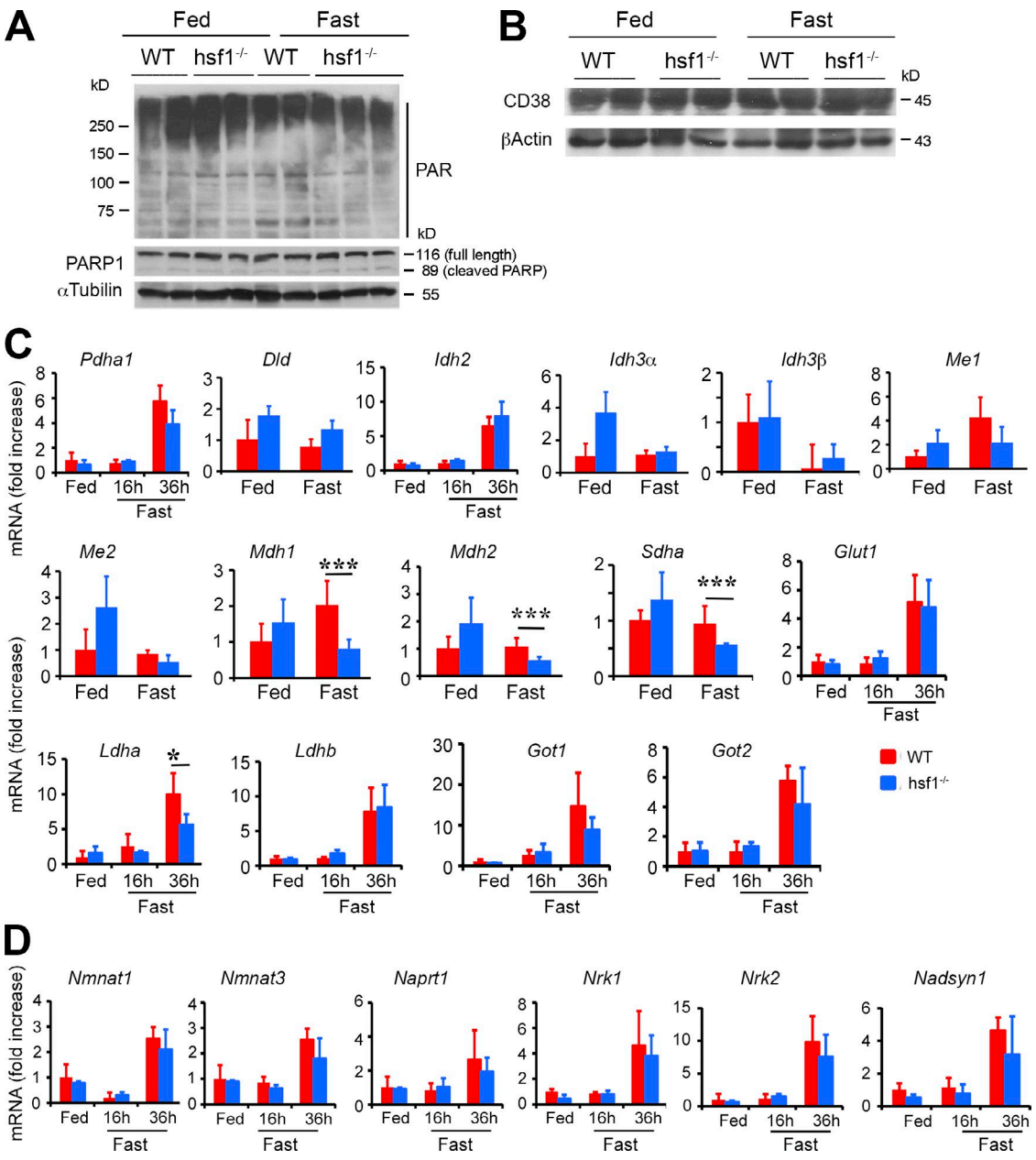

Figure S2. **Reduction of NAD⁺ levels by HSF1 loss is not caused by enhanced NAD⁺-consuming PARP activity or increased mRNA levels of dehydrogenases that reduce NAD⁺ to NADH.** (A) A representative experiment demonstrating no significant effect of *hsf1*-deletion on hepatic NAD⁺-consuming PARP activity. Total liver extracts from fed or fasted *hsf1*$^{-/-}$ mice and WT controls were analyzed by Western blot analysis for global protein PARylation and PARP-1 levels (from three individual experiments). (B) Representative Western blot analysis of CD38 protein levels in livers of *hsf1*$^{-/-}$ and WT mice during fed or 24-h fasted states (from three individual experiments). (C) Quantitative PCR of mRNA transcript levels of selected enzymes that regulate NAD⁺/NADH or NADP⁺/NADPH redox balance in livers of fed or fasted WT and *hsf1*$^{-/-}$ mice. In addition, the mRNA levels of Got1 and Got2 enzymes, which are major participants in the malate–aspartate shuttle, were not significantly different between genotypes. Values are presented as relative mRNA expression. Bars represent mean ± SD (n = 5 mice of each genotype). Statistical significance is indicated (*, $P < 0.05$; ***, $P < 0.001$). Bars indicate WT (red) or *hsf1*$^{-/-}$ (blue) mice. (D) mRNA levels of genes encoding enzymes in the NAD⁺ biosynthesis in the liver of fed or fasted WT and *hsf1*$^{-/-}$ mice. Data are presented as relative mRNA expression (n = 5 mice per group). For all panels, error bars show mean ± SD. *, $P < 0.05$; **, $P < 0.01$; ***, $P < 0.001$. Bars represent WT (red) or *hsf1*$^{-/-}$ (blue) mice.

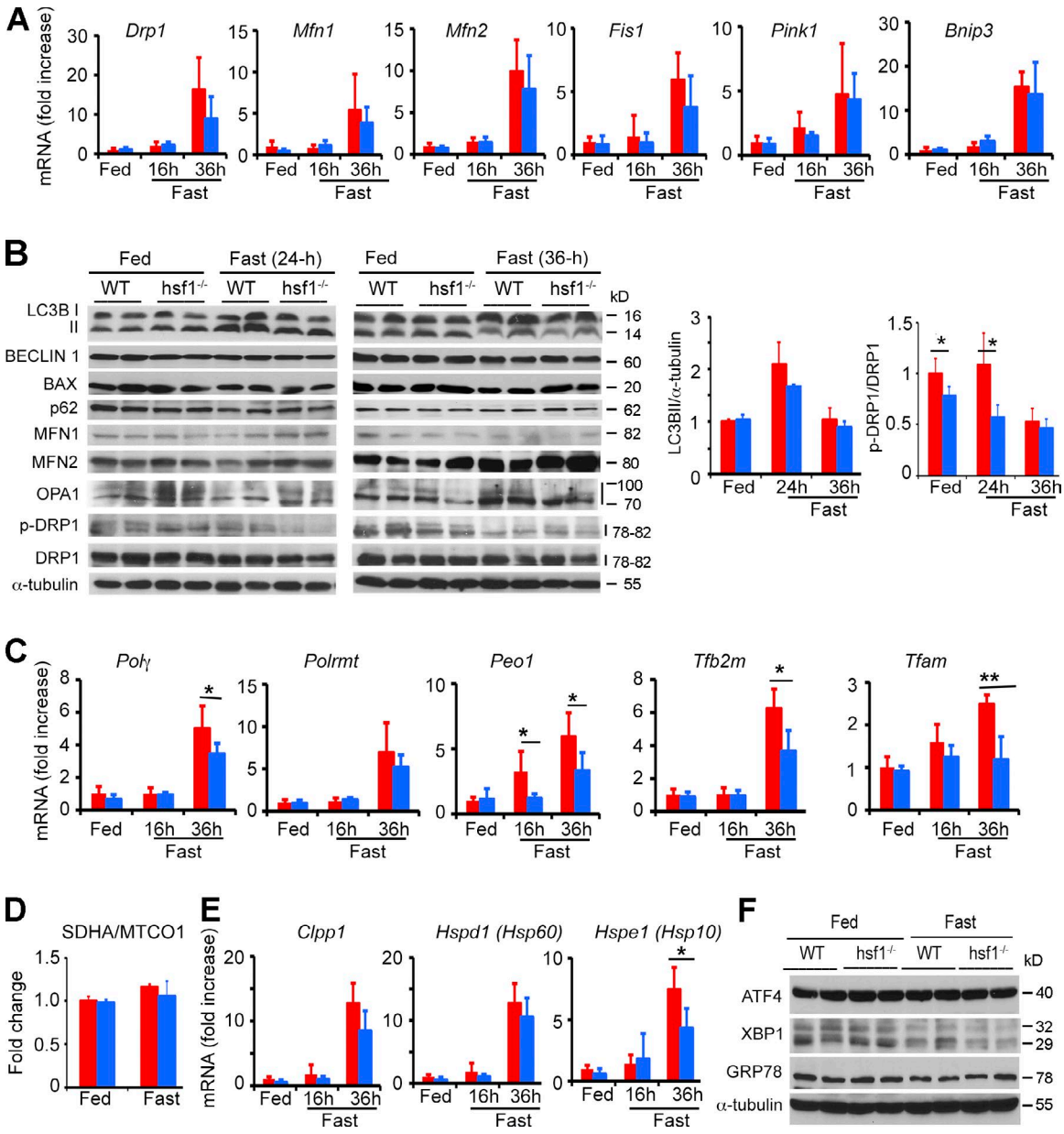

Figure S3. **Deletion of *hsf1* alters hepatic mitochondrial dynamics and biogenesis.** (A) Relative mRNA transcript abundance of genes regulating mitochondria dynamics and mitophagy in liver samples from fed or fasted (16 or 36 h) WT controls and *hsf1*$^{-/-}$ mice. (B) Relative level of indicated proteins involved in macroautophagy and mitochondrial fission or fusion in liver samples from fed or fasted WT and *hsf1*$^{-/-}$ mice. Graph shows quantification of LC3II that marks induction of autophagy versus α-tubulin protein levels as well as of the p-DRP1/DRP1 ratio that marks the induction of mitochondrial fission. (C) Relative mRNA expression levels of genes involved in mitochondrial DNA replication in livers of fed or fasted WT controls and *hsf1*$^{-/-}$ mice. (D–F) No apparent effects of *hsf1* deletion on mitonuclear protein balance and nutrient induced mitochondrial or ER unfolded protein (UPR) responses and autophagy. (D) Levels of mitochondrial (MT-CO1) or nuclear (SDHA) encoded proteins that define the mitonuclear balance in whole liver extracts from fed or 24-h fasted WT control and *hsf1*$^{-/-}$ mice. Graph shows quantification of SDHA/MT-CO1 ratio. (E) Hepatic mRNA transcript levels of UPR^{mit}-associated genes (e.g., *Clpp*, *Hspe1*, and *Hspd1* that encode for CLPP, HSP10, and HSP60 proteins, respectively). (F) Western blot analysis of selected proteins indicative of UPR^{ER} in liver samples from fed or fasted mice. α-Tubulin was used as a loading control. For all panels, error bars show mean ± SD (n = 4–5 mice of each genotype). Statistical significance is indicated (*, $P < 0.05$; **, $P < 0.01$). Bars indicate WT (red) or *hsf1*$^{-/-}$ (blue) mice.

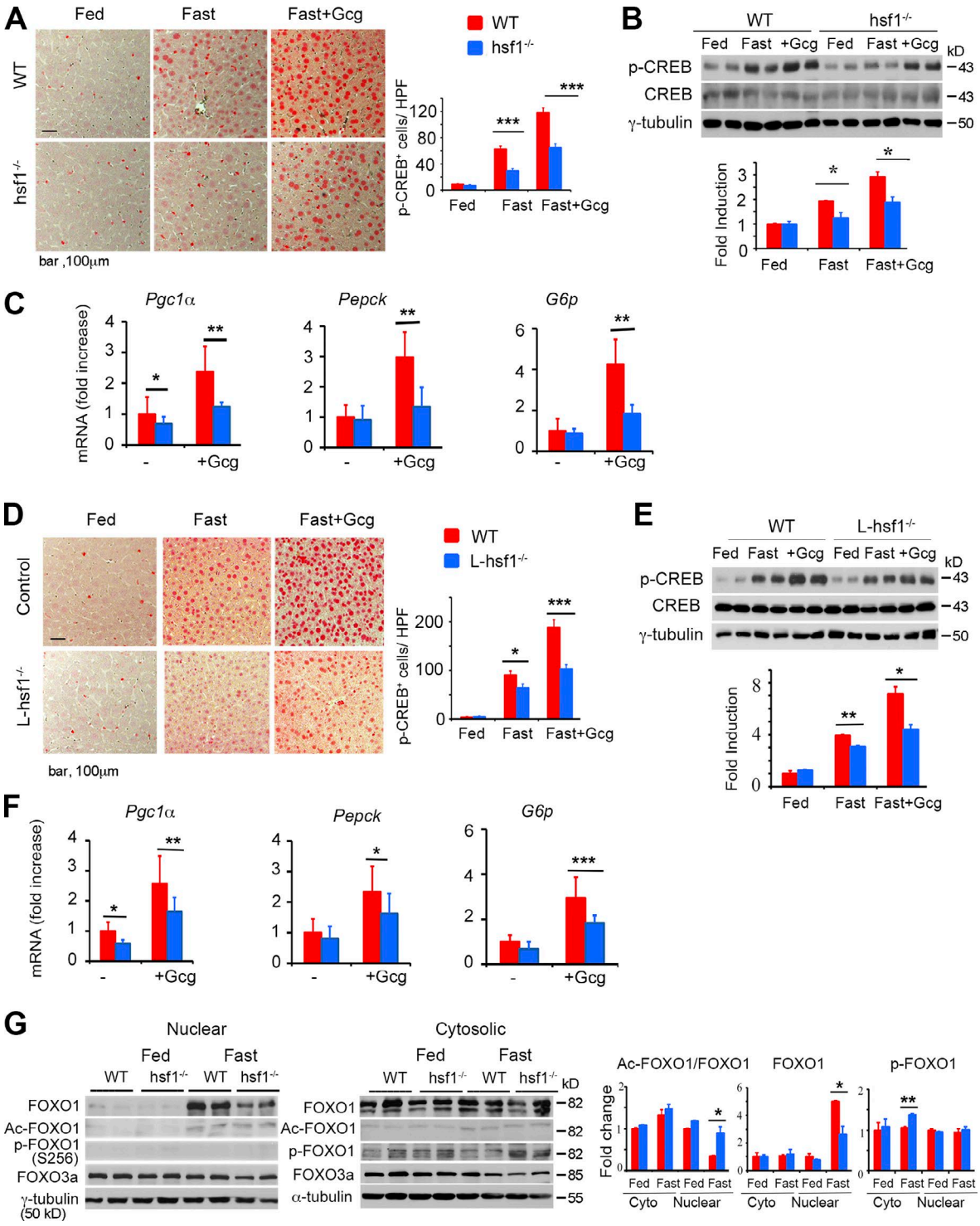

Figure S4. **Whole-body or hepatocyte-specific HSF1 ablation inhibits gluconeogenesis through attenuation of glucagon response and nuclear exclusion and inactivation of FOXO1 activity.** (A and B) Immunohistochemical staining (A) and Western blot analysis (B) showing effects of glucagon (30 µg/kg body weight) or saline injection on p-CREB (S133) localization and nuclear protein levels in livers prepared from fed or 4-h fasted WT controls and *hsf1*$^{-/-}$ mice. Notably, for this study, the animals were euthanized 10 min after glucagon (Gcg) injection via the inferior cava. Graphs show quantification of p-CREB–positive cells per high-power field (HPF; bar, 100 µM) or relative protein levels of p-CREB normalized to total CREB and expressed as relative fold-increase to control (WT fed without glucagon) that was arbitrarily set at 1 (below). (C) mRNA transcript levels of selected glucagon-induced genes involved in gluconeogenesis in livers of mice treated as described in A. (D–F) IHC staining (D), Western blot (E), and mRNA transcript expression (F) analyses as described in A–C were performed with glucagon-treated or untreated WT controls and L-*hsf1*$^{-/-}$ mice. (G) Fasting induced FOXO1 nuclear translocation in livers. Western blot analysis for acetylated (Ac) FOXO1, p-FOXO1 (S256), FOXO1, or FOXO3a in cytosolic and nuclear fractions from fed or 24-h fasted WT and *hsf1*$^{-/-}$ mice. FOXO1 acetylation in liver extracts was determined by direct Western blotting with antibody to acetyl-FRKH (Ac-FOXO1). Bar graphs quantitate relative Ac-FOXO1 or p-FOXO1 levels normalized to total FOXO1. In addition, the ratio of FOXO1 level normalized to loading control in the cytosolic or nuclear extracts of WT and *hsf1*$^{-/-}$ mice is indicated. For all panels, bars represent mean ± SD (*n* = 4–6 mice of each genotype). Statistical significance is indicated (*, P < 0.05; **, P < 0.01; ***, P < 0.001).

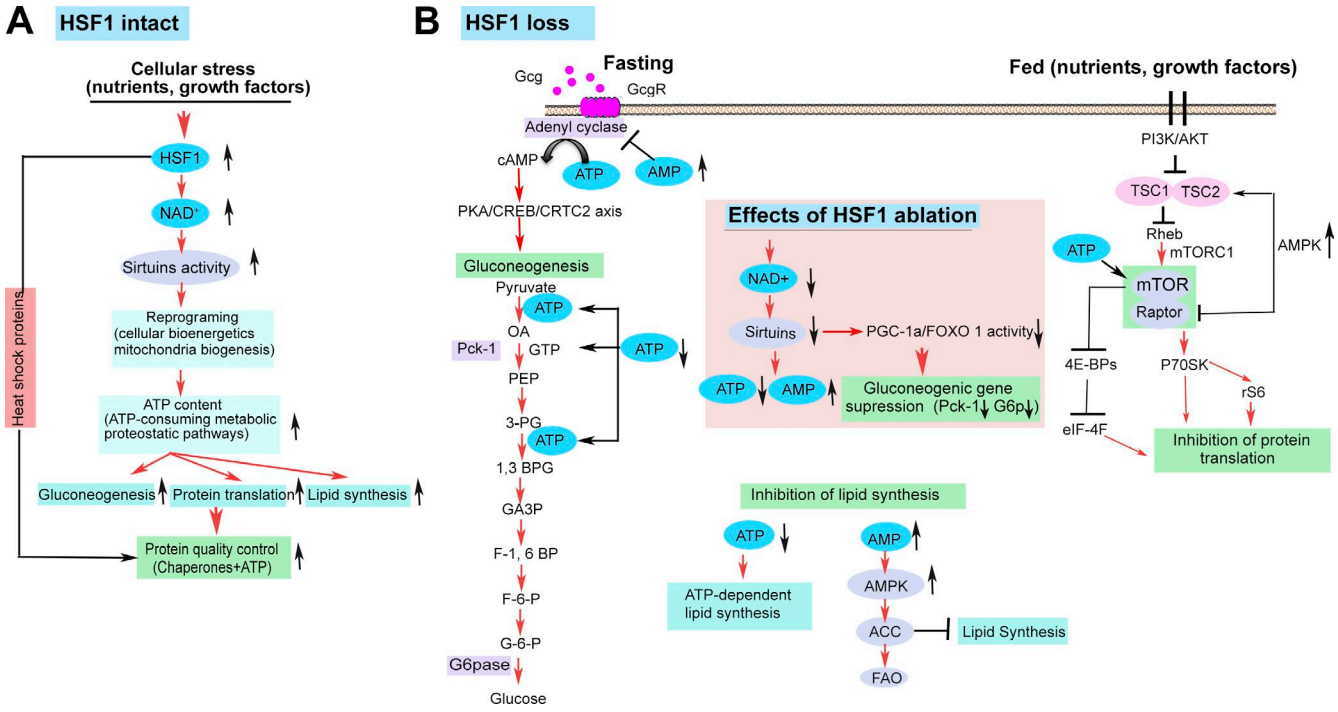

Figure S5. **Model depicting the mechanism by which HSF1 regulates hepatic energy and metabolic efficiency.** The figure summarizes some of the major findings of this study. Accordingly, HSF1 acts as a central information node of a transcription regulatory network that monitors perturbations in NAD^+ and ATP pools and reprograms mitochondrial activity that increases translational, bioenergetics, and metabolic efficiency to ensure cell survival under stress conditions. (A) Our study suggests that HSF1 activation by a variety of stressors, including nutrient-induced protein translation, plays at least two critical roles: monitoring the cytosolic protein folding state by inducing heat shock proteins and optimizing NAD^+ biosynthesis, cellular NAD^+ pools, and the NAD^+/NADH ratio linked to stimulation of sirtuin deacetylase activity and reprogramming of nuclear and mitochondrial acetylome to increase energetic efficiency and ATP regeneration. These nonexclusive functions of HSF1 activity are precisely balanced under fluctuating nutrient conditions. During an excess of nutrient supplies with the greatest metabolic and protein translation burden, HSF1 facilitates optimal metabolic homeostasis associated with large amounts of ATP consumption by supporting ATP regeneration and anabolic metabolic processes. Notably, as supported by transcriptome sequencing analyses, the marked increase in nuclear HSF1 activity during refeeding appears to be preferentially consumed, supporting the amplification of nutrient-induced translational and heat shock protein gene expression. In contrast, the attenuation of translation and the absence of heat shock protein response during fasting that decreases the overall demand of HSF1 activity could provoke a relative shift of HSF1 activity toward the transcription of energy-regulating genes, including NAMPT. Thus, a shift in hepatic transcriptional activity of HSF1 during the fed versus fasted state may compensate for the limited nuclear availability of HSF1 during fasting. Although a dramatic decrease in protein translation and lipid synthesis during fasting limits competition for energy resources, gluconeogenesis, a dominant function of hepatic cells, is a driving force for ATP consumption. We propose, in this situation, that the cell readily adapts to this relatively increased energetic demand by maximizing the use of limited resources for ATP regeneration, a process particularly aided by HSF1-dependent regulation of NAD^+ biosynthesis. (B) In the absence of HSF1, hepatic cells efficiently adapt their basal energetic profile to nutrient signaling fluctuation by down-modulating pathways regulating protein synthesis, lipid synthesis, and gluconeogenesis. In the context of physiological function and disease, these compensatory changes have beneficial effects, preventing diabetes and obesity, and can even explain the tumor-inhibitory effects of HSF1 ablation, but a lower ATP level may limit the protein-folding capacity and potentiate the development of degenerative diseases. Mechanistically, the inhibition of sirtuin activity as invoked by decreased NAD^+ levels and a lower NAD^+/NADH ratio alters the protein acetylation status in the liver and promotes the induction of a program of metabolic adaption. We postulate that changes in acetylation status of metabolic enzymes in the cytosolic and nuclear pools, and proteins that regulate mitochondrial DNA replication and biogenesis, including TFAM, PGC-1α, and FOXO1, can cause a dramatic decrease in total ATP regenerative capacity. The decrease in ATP levels is accompanied by higher levels of AMP and an increased AMP-to-ATP ratio, and these alterations have several critical roles in changing the metabolic activity of hepatic cells and stimulating energy-saving programs. First, the decrease in ATP levels impacts the rate of hepatic glucose production by decreasing the activity of ATP-dependent gluconeogenic enzymes. A deficit in the intracellular ATP pool similarly affects protein translation rates by directly suppressing mTORC1 activity. It is also possible that HSF1 ablation has an attenuating effect on lipid synthesis by inhibiting ATP-dependent metabolic steps. Second, the effect of HSF1 ablation on increased AMP levels and changes in the AMP-to-ATP ratio disrupts glucagon-stimulated cAMP–PKA signaling through allosteric inhibition of adenylyl cyclase and thereby inhibits gluconeogenic gene transcription and glucose output rates. Third, activation of AMPK, which detects elevated AMP levels, suppress translation by down-modulating mTORC1 activity and exerts insulin-sensitizing and lipid synthesis inhibitory effects. Fourth, the inhibitory effect of HSF1 loss on glucose production capacity is potentiated by acetylation and nuclear exclusion of FOXO1, which has an important role in controlling glucose output under fasting conditions. Thus, *hsf1* deficiency counteracts energy-consuming anabolic pathways to increase metabolic efficiency under nutrient-limiting stress conditions and ensures cell survival. By stimulating transcription of stress-related mRNAs that encode both chaperone proteins and genes of adaptive energetic and metabolic pathways, HSF1 thus provides sufficient energy (ATP and NAD^+) for protein synthesis and protein-folding capacity. Our data establish HSF1 as an energy sensor that integrates cellular protein and metabolic functions with bioenergetics.

Table S1. **Primers used for quantitative real-time PCR**

Gene name	Forward primer (5′ to 3′)	Reverse primer (5′ to 3′)
Atp5j	GTCCGGTCGCAGACTCCCTT	GCCGCCACCGTTCTACTTCC
Atp6	CAGTCCCCTCCCTAGGACTT	TCAGAGCATTGGCCATAGAA
MT-Co2	TGCTTGATTTAGTCGGCCTGGGAT	ACCTGGTGAACTACGACTGCTAGA
Cox5b	GTGCAGCCAAAACCAGATGA	AGAAGGGACTGGACCCATACAA
Clpp	TGTTGCGGGAACGCATCGTGT	AGATGGCCAGGCCCGCAGTT
Dld	GAGCTGGAGTCGTGTGTACC	CCTATCACTGTCACGTCAGCC
Drp1	CTGACACTTGTGGATTTACC	CCCTTCCCATCAATACATCC
Erra	GCAGGGCAGTGGGAAGCTA	CCTCTTGAAGAAGGCTTTGCA
FIS-1	ACTGAGCCCCAGAACAAC	TCAGGATTTGGACTTGGAG
Got1	GGGTAAAGGTGCCGTTCACAGT	GGGCGATGGTACAATGGTACAG
Got2	GGACCTCCAGATCCCATCCT	GGTTTTCCGTTATCATCCCGGTA
Glud1	CCCAACTTCTTCAAGATGGTGG	AGAGGCTCAACACATGGTTGC
G6p	TGGGCAAAATGGCAAGGA	TCTGCCCCAGGAATCAAAAAT
Hsp70	AGGTGCTGGACAAGTGCCAG	AACTCCTCCTTGTCGGCCA
Hspe1	CTGACAGGTTCAATCTCTCCAC	AGGTGGCATTATGCTTCCAG
Hspd1	GCTGTAGCTGTTACAATGGGG	TGACTTTGCAACAGTGACCC
Idh1	GGAGAAGCCGGTAGTGGAGAT	GGTCTGGTCACGGTTTGGAA
Idh3a	TGGGTGTCCAAGGTCTCTC	CTCCCACTGAATAGGTGCTTTG
Idh3b	TGGAGAGGTCTCGGAACATCT	AGCCTTGAACACTTCCTTGAC
Ldha	TGTCTCCAGCAAAGACTACTGT	GACTGTACTTGACAATGTTGGGA
Ldhb	CATTGCGTCCGTTGCAGATG	GGAGGAACAAGCTCCCGTG
Me1	GATGATAAGGTCTTCCTCACC	TTACTGGTTGACTTTGGTCTGT
Me2	TTCTTAGAAG CTGCAAAGGC	TCAGTGGGGAAGCTTCTCTT
Mdh1	TTCTGGACGGTGTCCTGATG	TTTCACATTGGCTTTCAGTAGGT
Mdh2	CGATATCGCTCACACACCTG	CGTGTCATTCCTGGTTTCCT
Mfn-1	AGCCCCAACATCTTCATTCTGAA	CTTACAACCTTGAGCTCTTCTACCA
Mfn-2	CATCAGTTACACCGGCTCTAACT	GAGCCTCGACTTTCTTGTTCA
Nampt	GCAGAAGCCGAGTTCAACATC	TTTTCACGGCATTCAAAGTAGGA
Nd1	ATCGTTGAACAAACGAACCA	GGGATAACAGCGCAATCCTA
Nmnat-1	TGGCTCTTTTAACCCCATCAC	TCTTCTTGTACGCATCACCGA
Nmnat3	CCTGTGGTTCCTTCAACCCC	AGATGATGCCCTCAATCACCT
Naprt1	TGCTCACCGACCTCTATCAGG	CGAAGGAGCCTCCGAAAGG
Nrk1	ATGCACAGAGGGTCAGTTCC	CGCAGAAGCATACACAGCAT
Nrk2	GTCCTGCAACCAGCATACCT	GAGTTCCAGGACAGCCAGAG
Nadsyn1	ACGGCTGCTCACTACTTGTTA	CTGAGAACCGAGGCAACTTC
Nrf1	GGTCTCTCCCACAAGAGTGC	GGTGGGGGACAGATAGTCCT
Nrf2	TTCTTTCAGCAGCATCCTCTCCAC	ACAGCCTTCAATAGTCCCGT
Ppara	GGGTACACTACGGAGTTCACG	CAGACAGGCACTTGTGAAAACG
Pparg1a	AGCCGTGACCACTGACAACGAG	GCTGCATGGTTCTGAGTGCTAAG
Ppargc1b	GCCTCTCCAGGCAGGTTCA	TAGAGAACTCAGTCCAGAAGGCTTT
Pepck	CCACAGCTGCTGCAGAACA	GAAGGGTCGCATGGCAAA
Pdha1	GGGACGTCTGTTGAGAGAGC	TGTGTCCATGGTAGCGGTAA
Polg	AATGGTCCAGCGATCTCATC	GCTGCTGGAAAACCTCAAAG
Polrmt	TCTTCAAAAGTCTACAGGAGATGTTCAC	TGAGGTTGGCACTCTCAGTCA
Peo1	TTCTCCGACGTGCATATCCC	GCGCTTCTTTTCTGTACCTTCT
Sdha	TTGATGCTGTGGTTGTAGGC	CTCTTCCATGTTCCCCAGAG
Tfb2m	AGAGCCGTTGCCTGATTCTG	CCGATCGATTCCTGGATGTC
Tfam	CCAAGACTTCATTTCATTGTCG	CAGGAGGCAAAGGATGATTC

Table S2. **List of genes mentioned in the text**

Abbreviation	Gene name
ATP5J	ATP synthase–coupling factor 6, mitochondrial
ATP6	ATP synthase F_o subunit 6 (or subunit/chain A)
MT-CO2	Cytochrome *c* oxidase subunit 2
COX5B	Cytochrome *c* oxidase subunit 5B, mitochondrial
DLD	Dihydrolipoamide dehydrogenase
DRP1	Dynamin related protein 1
ERRA	Estrogen-related receptor α
FIS-1	Mitochondrial fission 1 protein
G6P	Glucose-6-phosphate dehydrogenase
GOT1	Aspartate aminotransferase, cytoplasmic 1
GOT2	Aspartate aminotransferase, cytoplasmic 2
GLUD1	Glutamate dehydrogenase 1
HSP70	Heat shock protein 70
IDH2	Isocitrate dehydrogenase 2 [NADP], mitochondrial
IDH3A	Isocitrate dehydrogenase [NAD] subunit α, mitochondrial
IDH3B	Isocitrate dehydrogenase [NAD] subunit β, mitochondrial
LDHA	Lactate dehydrogenase A
LDHB	Lactate dehydrogenase B
ME1	Malic enzyme 1
ME2	Malic enzyme 2
MDH1	Malate dehydrogenase 1, cytoplasmic
MDH2	Malate dehydrogenase 2, mitochondrial
MFN-1	Mitofusin-1
MFN-2	Mitofusin-2
NAMPT	Nicotinamide phosphoribosyltransferase
ND1	NADH-ubiquinone oxidoreductase chain 1
NMNAT-1	Nicotinamide mononucleotide adenylyltransferase 1
NMNAT-2	Nicotinamide mononucleotide adenylyltransferase 2
NAPRT1	Nicotinate phosphoribosyltransferase 1
NRK1	Nik-related kinase 1
NRK2	Nik-related kinase 1
NADSYN1	NAD(+) synthetase 1
NRF1	Nuclear respiratory factor 1
NRF2	Nuclear respiratory factor 2
SDHA	Succinate dehydrogenase complex, subunit A
PGC-1α	Peroxisome proliferator-activated receptor γ coactivator 1-α (Pprgc1a gene)
PGC-1β	Peroxisome proliferator-activated receptor γ coactivator 1-β (Pprgc1b gene)
PPARα	Peroxisome proliferator-activated receptor-α
PEPCK	Phosphoenolpyruvate carboxykinase
PDHA1	Pyruvate dehydrogenase E1 component subunit α, mitochondrial
PEO1	Progressive external ophthalmoplegia 1 protein; Twinkle protein, mitochondrial
POLG	DNA polymerase subunit γ
POLRMT	Polymerase (RNA) mitochondrial (DNA directed)
TFB2M	Transcription factor B2, mitochondrial
TFAM	Transcription factor A, mitochondrial
Reagents	
Carbonyl cyanide *m*-chlorophenyl hydrazone	Carbonyl cyanide *m*-chlorophenyl hydrazone (an ionophore that allows protons to cross the mitochondrial inner membrane)
Bt2-cAMP	A membrane-permeable analogue of cAMP (28745; EMD Millipore)